On the Mechanism of Ion Transport through Polyphosphazene Solid Polymer Electrolytes: NMR, IR, and Raman Spectroscopic Studies and Computational Analysis of ^{15}N-Labeled Polyphosphazenes

Thomas A. Luther,* Frederick F. Stewart, Joanne L. Budzien, Randall A. LaViolette, William F. Bauer, and Mason K. Harrup

Idaho National Engineering and Environmental Laboratory, P.O. Box 1625, Idaho Falls, Idaho 83415-2208

Christopher W. Allen and Azzam Elayan

The University of Vermont, Department of Chemistry, Cook Physical Sciences Building, Burlington, Vermont 05405

Received: December 6, 2002; In Final Form: February 11, 2003

Comprehensive investigation of lithium ion complexation with ^{15}N-labeled polyphosphazenes— ^{15}*N*-poly-[bis(2-(2-methoxyethoxy)ethoxy)phosphazene] (^{15}*N*-MEEP) and ^{15}*N*-poly-[((2-allylphenoxy)$_{0.12}$(4-methoxyphenoxy)$_{1.02}$(2-(2-methoxyethoxy)ethoxy)$_{0.86}$)phosphazene] (^{15}*N*-HPP)—was performed by NMR, IR, and Raman spectroscopies. Previous studies characterized the ionic transport through the polymer matrix in terms of "jumps" between neighboring polymer strands utilizing the electron lone pairs of the etherial oxygen nuclei with the nitrogen nuclei on the polyphosphazene backbone not involved. However, noteworthy changes were observed in the NMR, IR, and Raman spectra with the addition of lithium trifluoromethanesulfonate (LiOTf) to the polyphosphazenes. The data indicate that the preferred association for the lithium ion with the polymer is with the nitrogen nuclei, resulting in the formation of a "pocket" with the pendant groups folding around the backbone. NMR temperature-dependent spin−lattice relaxation (T_1) studies (^{13}C, ^{31}P, and ^{15}N) indicate significant lithium ion interaction with the backbone nitrogen nuclei. These studies are in agreement with molecular dynamics simulations investigating lithium ion movement within the polyphosphazene matrix.

Introduction

Important criteria for facile ion transport in a solid polymer electrolyte (SPE) include a low glass-transition temperature, available coordination sites, and internal flexibility at the molecular level.[1] These properties are readily accessible in polyphosphazene materials through synthetic adaptation. The first polyphosphazene material shown to have ion conducting properties when complexed with a metal salt was poly[bis(2-(2-methoxyethoxy)ethoxy)phosphazene] (MEEP) in 1984.[2] The understanding of the ionic interactions between a metal salt and a SPE matrix or the additive in a gel-based electrolyte is crucial to the development of efficient battery materials. The mechanism of ion transport in a polymer matrix has been studied intensely ever since the discovery of ionic conduction in poly(ethylene oxide) (PEO).[3] Primarily, infrared, Raman, and NMR spectroscopic and molecular modeling studies have focused on ionic transport through PEO and PEO-related materials.[1,4−7] These studies characterize the ionic transport through the polymer matrix in terms of "jumps" between neighboring polymer strands utilizing the electron lone pairs of the oxygen nuclei. The proposed transport of the metal ions through the MEEP matrix has been modeled on the PEO transport mechanism using the ether oxygen nuclei of the pendant groups and states that the backbone nitrogen nuclei are probably not involved in the coordination of the metal ion.[8]

There have been several examples that the backbone nitrogen nuclei in polyphosphazenes are not necessarily inert to coordination chemistry. In a recent cross-linking study, electron-beam radiation, thermally induced free radical, and metal ion complexation methods were utilized to investigate cross-linking between polymer strands in selected polyphosphazenes including MEEP.[9] The data show that increases in cross-link density achieved through radiation or thermal methods do not affect the glass transition temperature T_g of the polymer. However, lithium ion complexation with these polyphosphazenes results in a marked increase in the T_g. The increase in the T_g is attributed to an increase in the barrier to rotation about the nitrogen−phosphorus bond resulting from lithium ion coordination with the backbone nitrogen nuclei and not to the formation of interstrand ionic cross-links.[9]

A study of poly(methylphenylphosphazene) and poly(dimethylphosphazene) examined the tendency of polyphosphazenes to coordinate with various Lewis acids.[10] Wisian-Neilson and co-workers reported the preparation of soluble proton, silver, and lithium complexes and also a platinum dichloride complex with these nonpolyether polyphosphazenes. The ^{31}P NMR data for these complexes exhibited increasing downfield chemical shift changes of the phosphorus resonance associated with increasing concentrations of the added Lewis acids indicating complexation at the backbone nitrogen nuclei. Recent research utilizing poly(methylphenylphosphazene) in the synthesis of gold nanoparticles supports the basicity of the

* Corresponding author. Phone: (208) 526-0203. Fax: (208) 526-8541. E-mail: luthta@inel.gov.

10.1021/jp027641w CCC: $25.00
Published on Web 03/15/2003

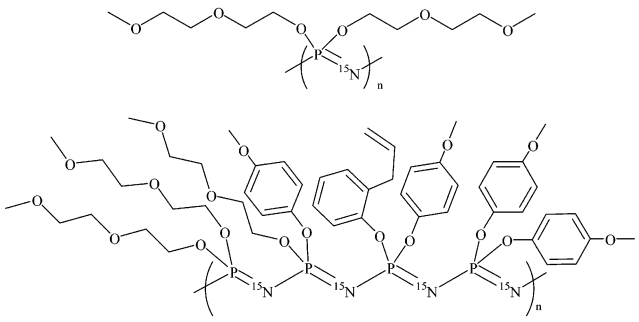

Figure 1. ^{15}N-poly[bis(2-(2-methoxyethoxy)ethoxy)phosphazene] (^{15}N-MEEP) (top) and ^{15}N-heteropolyphosphazene (^{15}N-HPP) (bottom) showing a representative section of the polymer with some of the possible random arrangements of the pendant groups.

nitrogen lone pair electrons on the inorganic backbone as a stabilizing influence controlling the size of the particles.[11]

Proton coordination to the backbone nitrogen has been confirmed by infrared spectroscopic studies involving polyphosphazene membranes that reported the observance of N−H stretches after these materials were treated with acid.[12,13] There is also X-ray crystallography data of a platinum complex with a phosphazene tetramer, $[N_4P_4(NHCH_3)_8]$, showing platinum nuclei bound to the backbone nitrogen exclusively.[14]

The current study was designed to specifically investigate lithium ion complexation in polyphosphazenes by NMR, IR, and Raman spectroscopies and by molecular dynamic simulation. Unfortunately, the natural abundance of the spin active ^{15}N nuclei is too low to be effectively studied by NMR spectroscopy (natural abundance ^{15}N is 0.35%). To overcome the natural abundance deficiency, two ^{15}N-labeled polyphosphazenes were synthesized— ^{15}N-poly[bis(2-(2-methoxyethoxy)-ethoxy)phosphazene] (^{15}N-MEEP) and a ^{15}N-heteropolyphosphazene (^{15}N-HPP)—consisting of regions conducive to ion transport, with 2-(2-methoxyethoxy)ethoxy pendant groups, along with regions where transport would be inhibited, predominately occupied by aryloxy pendant groups (Figure 1).

Experimental Section

Materials. NMR solvents tetrahydrofuran-d_8 (THF-d_8), deuterium oxide (D_2O), and chloroform-d ($CDCl_3$) were obtained from Cambridge Isotope Laboratories and used as received. Lithium trifluoromethanesulfonate (LiOTf), tetrahydrofuran (HPLC grade), and tetrabutylammonium bromide were purchased from Aldrich Chemical Co. and used as received. MEEP was prepared following literature procedures.[15]

NMR Spectroscopy. NMR data (^1H, ^{31}P, $^{13}C\{^1H\}$, and ^{15}N) were acquired on a Bruker DMX 300WB spectrometer with a magnetic field strength of 7.04 T corresponding to operating frequencies of 300.13 MHz (^1H), 121.49 MHz (^{31}P), 75.48 MHz (^{13}C), and 30.41 MHz (^{15}N). Additional NMR spectra were acquired on a Bruker DMX 750 spectrometer with a magnetic field strength of 17.63 T corresponding to operating frequencies of 750.13 MHz (^1H), 303.66 MHz (^{31}P), 188.64 MHz (^{13}C), and 76.01 MHz (^{15}N). The NMR spectra were referenced internally to TMS (^1H and $^{13}C\{^1H\}$) or externally to H_3PO_4 (^{31}P) or to $(^{15}NH_4)_2SO_4$ (^{15}N). Spin−lattice relaxation measurements were performed using standard inversion−recovery 180°-τ-90° pulse sequence experiments. Variable temperature NMR experiments were conducted using a Bruker DMX 300WB spectrometer equipped with a Bruker BVT 3000 temperature control module. Temperature calibration was accomplished by following the Van Geet methanol calibration method.[16]

IR Spectroscopy. Samples containing MEEP:Li and ^{15}N-MEEP:Li ratios of 1:0, 2:1, 1:1, and 1:2 were prepared gravimetrically using mer:LiOTf molar ratios. Infrared spectra were collected with a Bio-Rad FTS-65 Fourier transform infrared spectrometer with either a photoacoustic cell (MTEC Photoacoustics, model 300) or with an infrared microscope attachment (Spectra-Tech IR-Plan) operated in the reflection mode with a narrow-band MCT detector. The samples were loaded into aluminum pans and dried overnight in an argon vacuum oven at 125 Torr and 50 °C. The photoacoustic cell was purged with helium for several minutes prior to sealing the cell for data collection. Spectra were collected for each sample at rates of 2.5, 5, 10, and 20 kHz with 64, 128, 256, and 512 scans, respectively.

For the infrared microscopy, the samples were spotted onto gold coated slides and also dried overnight in an argon vacuum oven at 125 Torr and 50 °C. Spectra consisted of 64 coadded scans at 4 cm^{-1} resolution. For the FTIR−PAS measurements, the sample single-beam spectra were ratioed to the single-beam spectrum of carbon black. For the transflection spectra collected with the microscope attachment, the absorbance was calculated using the reflection spectrum from the gold-coated slide as a reference. For direct comparisons of spectra, all spectra were normalized by dividing by peak intensity from the CH_2 bending modes, $\delta(CH_2)$, of the MEEP ethoxy groups in the region of 1450−1470 cm^{-1}.[17,18]

Raman Spectroscopy. Raman spectra were collected on a Bruker Optics Equinox 55 FT spectrometer equipped with the FRA 106/s Raman module fiber-optically coupled to a microscope (RAMANSCOPE), a Si on CaF_2 beam splitter, and a high-sensitivity Ge detector. Each sample FT Raman spectrum consisted of 1024 coadded spectra at 8 cm^{-1} resolution. The samples were those spotted onto the gold-coated microscope slides. Spectra were normalized for evaluation as described above.

Molecular Weight Determination. The ^{15}N-polyphosphazenes were dissolved in a solution of THF containing 0.1 w/v % of tetrabutylammonium bromide and filtered through a 0.45 μm PTFE syringe filter prior to analysis. Solution refractive index increment (dn/dc) values were obtained using a Rainin Dynamax RI-1 differential refractive index (RI) detector. The detector constant was determined via calibration using known concentrations of polystyrene standards whose dn/dc values are well-known. Molecular weight and radius moments along with polydispersity indices were determined using a chromatographic system consisting of a Waters Alliance 2690 separations module, two Waters Styragel HR-5E solvent efficient columns (4.6 mm × 300 mm), a Rainin RI detector, and a Wyatt Technologies Dawn DSP laser-light-scattering detector. The light-scattering detector is equipped with a F2 flow-cell that measures scattered light intensities at 16 angles ranging from 12.3° to 165.1°.

Thermal Analysis. Glass transition temperatures were determined using a TA Instruments model 2910 differential scanning calorimeter and TGA analyses were performed using a TA Instruments model 2950 thermogravimetric analyzer.

Synthesis of ^{15}N-Polydichlorophosphazene. ^{15}N-Polydichlorophosphazene was produced from ^{15}N-labeled ammonium sulfate and PCl_5 following published procedures substituting ^{15}N-ammonium sulfate[19] for ^{14}N-ammonium sulfate.[20,21]

Synthesis of ^{15}N-Poly[bis(2-(2-methoxyethoxy)ethoxy)-phosphazene] (^{15}N-MEEP). ^{15}N-MEEP was generated by nucleophilic substitution of ^{15}N-polydichlorophosphazene utilizing sodium 2-(2-methoxyethoxy)ethoxide following published procedures for unlabeled MEEP.[15] ^1H NMR (THF-d_8) δ: 4.13

SCHEME 1

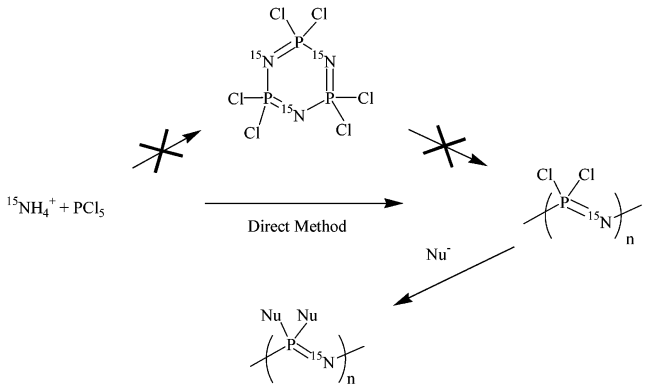

(br, 2H), 3.69 (2H, t, $J_{HH} = 5.0$ Hz), 3.64 (2H, t, $J_{HH} = 5.0$ Hz), 3.51 (2H, t, $J_{HH} = 4.9$ Hz), 3.33 (3H, s). $^{13}C\{^1H\}$ NMR (THF-d_8) δ: 73.1, 71.6, 71.3, 66.2, 59.2. ^{15}N NMR (THF-d_8) δ: 63.1. ^{31}P NMR (THF-d_8) δ: -6.7. Mw $= (1.60 \pm 0.02) \times 10^5$ g/mol, dn/d$c = 0.061$, RMS radius $= 49.9 \pm 0.5$ nm, PDI $= 1.20 \pm 0.02$.

Synthesis of ^{15}N-Poly[((2-allylphenoxy)$_{0.12}$(4-methoxyphenoxy)$_{1.02}$(2-(2-methoxyethoxy)ethoxy)$_{0.86}$)phosphazene] (^{15}N-HPP). ^{15}N-HPP was generated by nucleophilic substitution of ^{15}N-polydichlorophosphazene utilizing sodium salts of 2-(2-methoxyethoxy)ethanol (MEE), methoxyphenol (MeOP), and *o*-allylphenol (*o*-Al) generally following published procedures for a similar unlabeled heteropolyphosphazene.[22] ^1H NMR (300 MHz, THF-d_8) δ: 7.00, 6.66, 5.78, 4.92, 3.98, 3.63, 3.34, 3.26. $^{13}C\{^1H\}$ NMR (75.48 MHz, THF-d_8) δ: 157.0, 151.1, 146.5, 138.3, 132.6, 130.2, 127.9, 124.2, 123.2, 122.0, 116.0, 114.8, 72.8, 71.1, 66.1, 59.0, 55.6, 35.2. ^{15}N NMR (30.41 MHz, THF-d_8) δ: 68.2. ^{31}P NMR (121.49 MHz, THF-d_8) δ: -7.5, -12.1, -17.0. Mw $= (7.43 \pm 0.09) \times 10^4$ g/mol, dn/d$c = 0.108$, RMS radius $= 43.9 \pm 0.9$ nm, PDI $= 1.46 \pm 0.02$. DSC $T_g = -32$ °C, TGA $T_d = 302$ °C.

Results and Discussion

Synthesis and Characterization. Linear polyphosphazenes are generally synthesized by a low-yielding ring-opening polymerization of hexachlorocyclotriphosphazene to generate polydichlorophosphazene followed by addition of organic nucleophiles to the backbone.[23] To generate ^{15}N-polyphosphazenes, an alternate route was utilized where polydichlorophosphazene is formed directly from ammonium sulfate following published procedures.[20,21] ^{15}N-Ammonium sulfate was used in place of ^{14}N-ammonium sulfate (Scheme 1). Substitution reactions were then performed on the ^{15}N-polydichlorophosphazene using the appropriate sodium salts to generate ^{15}N-MEEP[15] and ^{15}N-HPP.[22] The structures of ^{15}N-MEEP and ^{15}N-HPP were verified by ^1H, ^{13}C, ^{15}N, and ^{31}P NMR spectroscopies, thermal analysis, and GPC. Additionally, a silver nitrate test resulted in no observable evidence for residual chloride present in ^{15}N-MEEP.

NMR Characterization. The NMR samples were typically prepared with approximately 300 mg ^{15}N-MEEP or ^{15}N-HPP and 1.0 mL solvent in a 5 mm NMR tube. The increased resolution and chemical shift dispersity observed with THF-d_8 as the solvent allows for the unambiguous assignment of the ^{13}C NMR resonances of the ^{15}N-MEEP polymer. The assignment of the carbon resonances of ^{15}N-MEEP via various NMR techniques including two-dimensional proton homonuclear (COSY) and proton−carbon heteronuclear (HETCOR) correlation experiments agree with published data for unlabeled MEEP.[8] The assignments are consistent with the results of NMR T_1 experiments where the relaxation times of carbon atoms in flexible side chains increase with distance from the polymer backbone due to the increased mobility (Figure 2).[24]

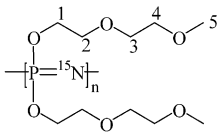

C1	C2	C3	C4	C5
0.30	0.37	0.78	1.13	3.61

Figure 2. ^{13}C spin−lattice relaxation times (T_1, s) for ^{15}N-MEEP ($CDCl_3$, 25 °C).

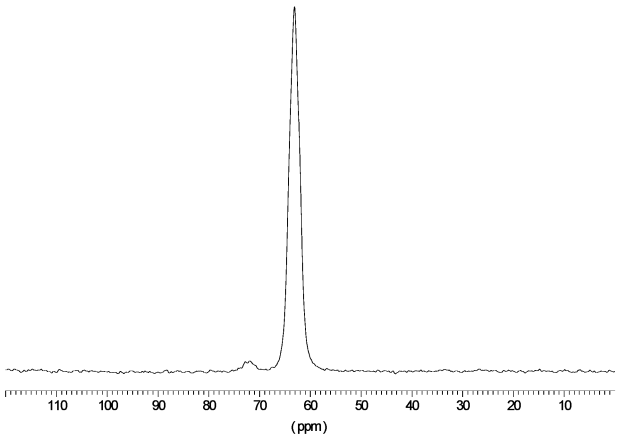

Figure 3. ^{15}N NMR spectrum of ^{15}N-MEEP (THF-d_8).

The ^{15}N NMR spectrum of ^{15}N-MEEP at an operating frequency of 30 MHz exhibits a major resonance at δ 63.1 (THF-d_8) with a full-width-at-half-maximum line width ($\Delta\nu_{1/2}$) of 75 Hz (Figure 3). A minor resonance that is evident in the ^{31}P NMR spectra downfield (0 to -5 ppm region) of the major resonance is also observed in the ^{15}N-NMR spectra (δ 71.9). Similar resonances are observed in the ^{31}P and ^{15}N NMR spectra of the related ^{15}N-HPP. These downfield resonances are attributed to polymer chain-end effects and to degradation products that develop with prolonged reaction times during the synthesis of polyphosphazenes.

Characterization of ^{15}N-HPP as ^{15}N-poly[((2-allylphenoxy)$_{0.12}$-(4-methoxyphenoxy)$_{1.02}$(2-(2-methoxyethoxy)ethoxy)$_{0.86}$)-phosphazene] was accomplished by integration of the ^1H NMR spectrum to determine the relative ratios of the pendant groups.[22] The ^{31}P NMR spectrum of ^{15}N-HPP acquired at an operating frequency of 121 MHz exhibits three resonances that are due to the phosphorus nuclei that have two MEE, one MEE and one aryloxy (OAr), or two OAr pendant groups attached.

The ^{15}N NMR spectrum of ^{15}N-HPP at 30 MHz is a single very broad resonance ($\Delta\nu_{1/2} \sim 260$ Hz). However, the ^{15}N NMR spectrum acquired at 76 MHz exhibits five separate resonances. These resonances correspond to the number of OAr pendant groups versus the number of MEE pendant groups attached to the adjacent phosphorus nuclei. When both neighboring phosphorus nuclei each have two OAr pendant groups attached, the ^{15}N resonance exhibits spin coupling of 40 Hz. As the number of aryloxy pendant groups decrease, the resolution decreases and the chemical shift of the resonance moves upfield. The ^{15}N resonance that is the furthest upfield has the immediate phosphorus environment similar to MEEP and has an observed chemical shift at approximately 62.3 ppm.

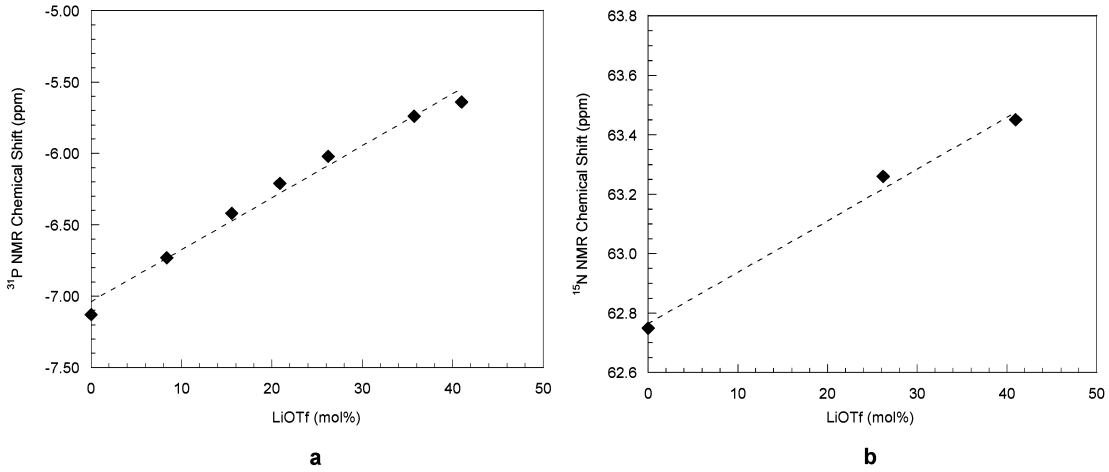

Figure 4. Change in the NMR chemical shift of ^{15}*N*-MEEP ($CDCl_3$) with the addition of LiOTf, (a) ^{31}P NMR (121 MHz), (b) ^{15}N NMR (30 MHz).

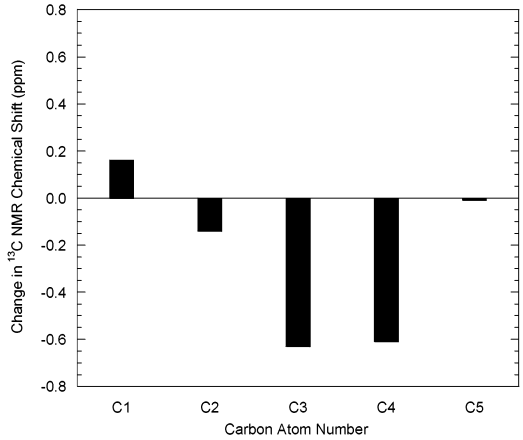

Figure 5. Change in $^{13}C\{^1H\}$ NMR chemical shifts for ^{15}*N*-MEEP in $CDCl_3$ after 39 mol % addition of LiOTf.

^{15}*N*-MEEP/Lithium Trifluoromethanesulfonate NMR Results. LiOTf was added to ^{15}*N*-MEEP in incremental amounts in an NMR tube. NMR spectra were acquired to observe chemical shift changes for the resonances of the ^{13}C, ^{31}P, and ^{15}N nuclei. LiOTf loadings of up to 106 mol % with respect to the polymer, resulted in no significant changes in the chemical shifts of the resonances with THF-d_8 as the solvent. This is an indication that the solvent−salt interactions dominate the polymer−salt interactions. At this solvent−polymer concentration, the number of available coordination sites favors the solvent over the oxygen and nitrogen nuclei of the polymer (approximately 2:1). Further NMR experiments were conducted using $CDCl_3$ since LiOTf is soluble in the polymer matrix but it is not appreciably soluble in $CDCl_3$. Amounts greater than 40 mol % addition of LiOTf resulted in incomplete solvation of the metal salt.

The observed chemical shift changes for the phosphorus resonance in the ^{31}P NMR spectra are consistent with lithium ion coordination occurring at either the adjacent oxygen nuclei or the nitrogen nuclei of the polymer backbone (Figure 4a). Similar reasoning can be used to describe the ^{15}N NMR chemical shift changes observed for the nitrogen resonance (Figure 4b). However, the observed chemical shift changes of the carbon resonances in the $^{13}C\{^1H\}$ NMR spectra do not support significant lithium ion coordination to the oxygen nuclei (Figure 5). Since the ^{31}P NMR spectra exhibit observable chemical shift changes with the addition of LiOTf, a significant chemical shift change for the C1 resonance should be observed if the lithium ions were coordinating to the oxygen nuclei that are bound to phosphorus. Additionally, if lithium ion coordination were occurring at the other oxygen nuclei in the pendant group, one would expect the observed chemical shift change for the C2 resonance to be similar to the chemical shift change for the C3 resonance. In addition, the C4 and C5 resonances would have similar chemical shift changes with respect to each other dependent upon which oxygen nuclei was the coordination site. The observed chemical shift changes are more consistent with lithium ion coordination with the nitrogen nuclei and the pendant groups folding around the backbone resulting in the formation of a "pocket" (Figure 6).

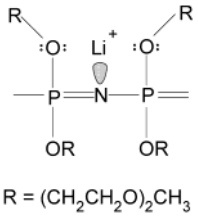

Figure 6. Lithium association with the nitrogen in polyphosphazenes. Note the chelating effect of the ligand oxygens forming a "pocket" directly on the backbone.

^{15}*N*-HPP/Lithium Trifluoromethanesulfonate NMR Results. The chemical shift changes observed in the ^{31}P NMR spectra due to increasing lithium ion concentration directly correspond to the number of MEE pendant groups attached to the phosphorus nuclei (Figure 7). The resonance of the C4 carbon in the MEE pendant group in the $^{13}C\{^1H\}$ NMR spectra of ^{15}*N*-HPP after the addition of LiOTf exhibits a chemical shift change of −0.6 ppm. The other carbon resonances exhibit smaller chemical shift changes, in the −0.2 to 0.2 ppm range along with the carbon resonances of the methoxyphenoxy and *o*-allylphenoxy pendant groups. The ^{15}N NMR spectrum (76 MHz) of ^{15}*N*-HPP after the 39 mol % addition of LiOTf exhibits observable decreases in the resolution of resonances B−D and a downfield shift of ∼1 ppm for resonance E (Figure 8). Resonance A with four OAr pendant groups attached to the adjacent phosphorus nuclei does not undergo any observable change. The NMR data for ^{15}*N*-HPP indicate lithium ion association is more readily facilitated when the nitrogen nucleus is surrounded by four MEE pendant groups on the adjacent phosphorus nuclei. This is also consistent with the observations seen in ^{15}*N*-MEEP regarding the formation of a "pocket" that allows association of the lithium ion with the backbone nitrogen nuclei.

Temperature Dependence of Spin−Lattice Relaxation. The spin−lattice relaxation rate is comprised of various contributions

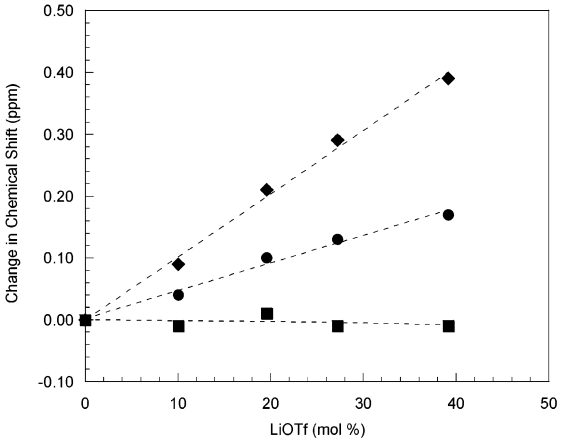

Figure 7. Change in ^{31}P NMR chemical shifts of ^{15}N-HPP ($CDCl_3$, 121 MHz) with increasing amounts of LiOTf. The symbols correspond to the following pendant group configurations attached to the phosphorus nuclei: ♦ = $(MEE)_2$, ● = (MEE)(OAr), ■ = $(OAr)_2$.

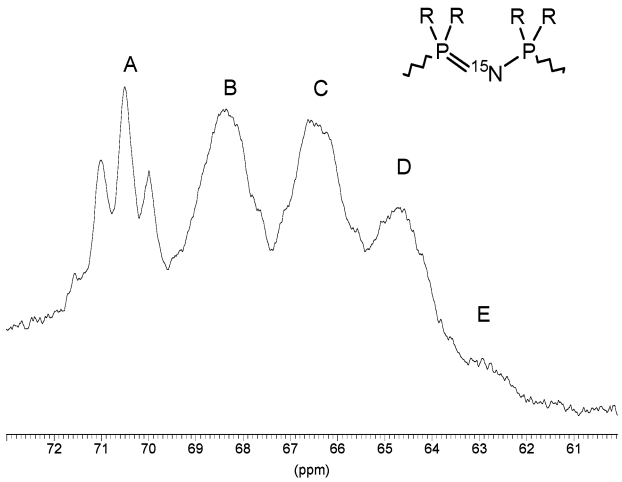

Figure 8. ^{15}N NMR spectrum of ^{15}N-HPP after 39 mol % addition of LiOTf ($CDCl_3$, 76 MHz). The pendant group assignments for the observed resonances are A: R = four OAr. B: R = three OAr and one MEE. C: R = two OAr and two MEE. D: R = one OAr and three MEE. E: R = four MEE.

to the relaxation process, including homo- and heteronuclear dipolar interactions, quadrupolar interactions, chemical shift anisotropy, spin-rotation, and others.[25] When the relaxation mechanism is dominated by inter- and intramolecular dipole−dipole interactions, the relaxation rate will increase with temperature, pass through a maximum, and decrease with increasing temperature. Since T_1 is the inverse of the relaxation rate, it will decrease, pass through a minimum, and then increase with increasing temperature.[26] The minimum value of the spin−lattice relaxation time (T_{1min}) is proportional to the internuclear distances.

The addition of LiOTf to ion-conducting polyphosphazenes results in a decrease in the flexibility of the polymer exhibited by an increase in T_g.[27] It was reported that this decreased flexibility may result from ionic cross-links between polymer strands through the etherial oxygen nuclei in the pendant groups.[28] However, a recent study showed that when MEEP is fully cross-linked through electron beam irradiation, there is no significant change in T_g.[9] The decrease in polymer flexibility upon addition of LiOTf is also observed as an increase in temperature where T_{1min} occurs. Temperature-dependent T_1 values of ^{15}N-MEEP in $CDCl_3$ were measured for the internal

TABLE 1: $^{13}C\{^1H\}$ NMR Spin−Lattice Relaxation Minimum Values (T_{1min}) of ^{15}N-MEEP ($CDCl_3$, 75 MHz) before and after LiOTf Complexation (s, °C)

	C1	C2	C3	C4	C5
^{15}N-MEEP	0.11,−47	0.11,−47	0.15,−58[a]	0.16,−58[a]	0.58,−58[a]
^{15}N-MEEP/Li^+	0.15,12	0.15,12	0.22,12	0.23,12	1.30,−11[a]

[a] The measurable T_1 had not reached a minimum value at the lowest temperature recorded.

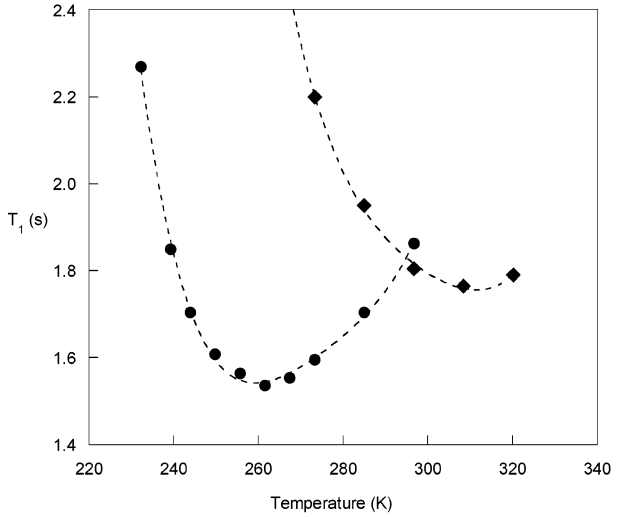

Figure 9. ^{31}P NMR variable temperature spin−lattice relaxation of ^{15}N-MEEP ($CDCl_3$, 121 MHz) before and after addition of LiOTf. The symbols correspond to ● = ^{15}N-MEEP, ♦ = ^{15}N-MEEP + LiOTf.

spin = $^1/_2$ nuclei (^{13}C, ^{31}P, and ^{15}N) to explore the changes in T_{1min} values after the addition of LiOTf.

The $^{13}C\{^1H\}$ NMR temperature-dependent T_1 data of ^{15}N-MEEP are summarized in Table 1. Minimum values for the relaxation times were not obtainable for all the carbon nuclei due to extreme broadening of the resonances with decreasing temperatures. Before the addition of LiOTf, at the lowest temperature recorded (−58 °C), the T_1 for C3 had reached a constant value of 0.15 s and the T_1 for C4 was approaching a constant value. Only the C5 resonance T_1 data was still decreasing sharply with the decrease in temperature. After the 39 mol % addition of LiOTf, minimum relaxation times were observed for all the nuclei except C5, which was still decreasing slightly at the lowest obtainable temperature. The T_{1min} values show increases in relaxation times of approximately 0.04 s for C1 and C2, and approximately 0.07 s for C3 and C4 with the addition of LiOTf.

The ^{31}P NMR temperature-dependent T_1 data of ^{15}N-MEEP indicate a T_{1min} value increase of 0.21 s after the addition of the LiOTf (Figure 9). However, the ^{15}N NMR T_{1min} value decreases significantly with the addition of LiOTf, from approximately 7.5 to 5.0 s (Figure 10). Since the T_{1min} value is proportional to the internuclear distance, an increase is expected when lithium ion complexation occurs at an adjacent nucleus. This is the result of an increase in the bond lengths caused by the decrease in the electron density of the preexisting bonds. The increases measured for the phosphorus and the C1 carbon nuclei T_{1min} values could be due to lithium ion complexation occurring at the first oxygen nuclei of the pendant groups. The slight increases in the other carbon nuclei T_{1min} values may also be attributable to lithium ion complexation to either the second or third oxygen nuclei. However, the marked decrease in the T_{1min} value of the ^{15}N resonance is only consistent with lithium ion coordination with the nitrogen nuclei and the additional

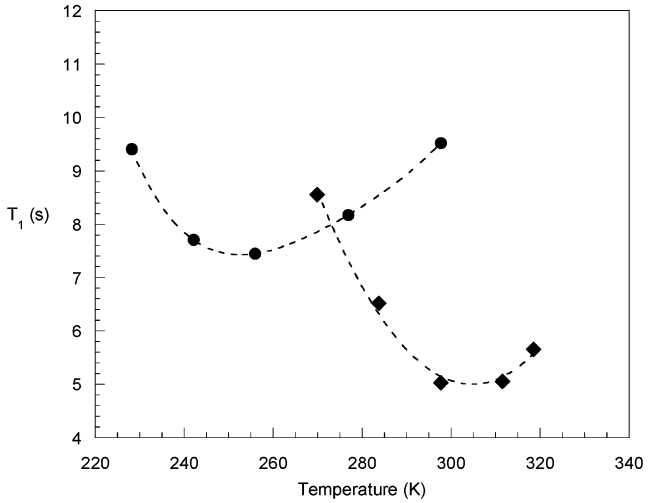

Figure 10. ^{15}N NMR variable temperature spin−lattice relaxation of ^{15}*N*-MEEP ($CDCl_3$, 30 MHz) before and after addition of LiOTf. The symbols correspond to ● = ^{15}*N*-MEEP, ♦ = ^{15}*N*-MEEP + LiOTf.

heteronuclear and quadrupolar interactions providing significant contributions to the relaxation process.

Infrared and Raman Spectroscopies. Previous studies employing vibrational spectroscopies to investigate solvents and polymer electrolytes containing dissolved LiOTf focused heavily upon the ionic state of the triflate anion. Many of these systems utilized solvents or polymers with multiple ether functionalities. Because of the relative complexity of the triflate anion spectrum, at higher triflate salt concentrations it tends to dominate the spectrum, making interpretation of the salt component effects on the polymer difficult. However, information concerning the interaction of the cation contributed by the triflate salt with the polymer have been inferred by examining the $\rho(CH_2)$ rocking motions of the −O−C−C−O− units in the 825−870 cm^{-1} region and attributing the changes in this region to changes in the tortional conformations due to the interaction of the cation with the ether oxygens of the polymer.[6] In one case, utilizing MEEP and LiOTf, there was also some indication of an effect of the cation on the P−O bending and/or P−N stretching modes seen in the Raman spectrum around 600−630 cm^{-1}.[29] This observation provides some evidence that the cation can interact with the polyphosphazene backbone in MEEP.

To provide more conclusive evidence of the interaction of the cation with the polyphosphazene backbone of MEEP using vibrational spectroscopy, ^{15}*N*-MEEP was directly compared to natural abundance (^{14}N) MEEP. The use of ^{15}N should cause a shift of ∼2.3% in any bands associated with the −N−P═N− backbone of MEEP. Samples containing MEEP:Li and ^{15}*N*-MEEP:Li ratios of 1:0, 2:1, 1:1, and 1:2 were prepared gravimetrically using mer:LiOTf molar ratios. Nearly identical spectra were obtained with the samples coated onto gold and with the photoacoustic cell, however, there was some inconsistency when thin films on gold were made due to chemical segregation associated with the solvent fronts. The expected spectral shift of 28.5 cm^{-1} from the published values[13] for the P═N bond at ∼1243 cm^{-1} to ∼1214 cm^{-1} is readily apparent (Figure 11). However, the remainder of the spectrum is highly overlapped and the addition of the lithium triflate salt complicates the spectrum considerably (Figure 12). The ionic environment of the triflate anion is readily apparent in the SO_2 deformation band[30] around 644 cm^{-1}. This band becomes significantly broader at increasing LiOTf concentrations and the peak maximum shifts from 644 cm^{-1} at MEEP:Li ratios of 2:1 to 652 cm^{-1} at MEEP:Li ratios of 1:2 (Figure 12b). The shift

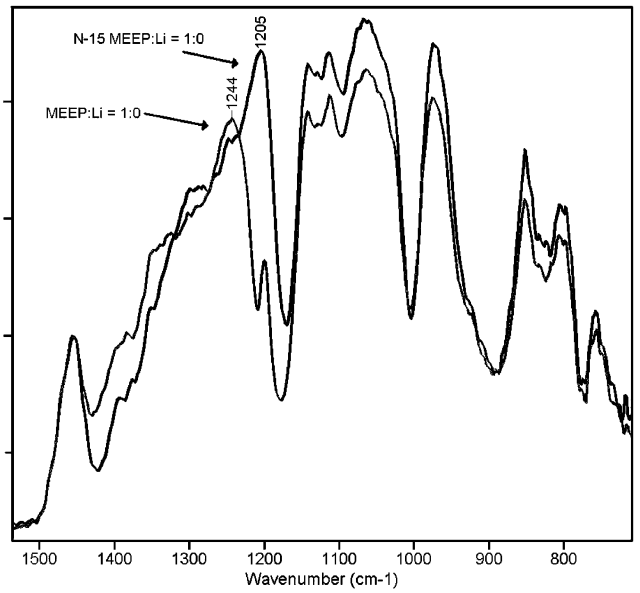

Figure 11. Infrared spectra of MEEP and ^{15}*N*-MEEP collected with a photoacoustic cell at a scan rate of 10 kHz.

and broadening of this band is consistent with the interpretations of the free ion, ion pair and "triple" anion ($Li(OTf)_2$) or aggregate as reported by others.[18,29,31] The "triple" anion is more likely a 1:1:1 complex of the triflate anion, lithium, and two ether oxygen atoms from the polymer side chains.[32]

To eliminate the similarities in the spectra and emphasize the differences in the ^{14}*N*-MEEP and ^{15}*N*-MEEP, the spectrum of ^{14}*N*-MEEP was ratioed to the spectrum of ^{15}*N*-MEEP at each of the MEEP:Li ratios (Figure 13). The differences are fairly consistent in the 1455−1327 cm^{-1} range and at 1003 cm^{-1} where there are likely some small changes in the P−O−C bonding associated with minor changes in the bond lengths between the P and N atoms. The changes in the 1200 cm^{-1} range, however, directly reflect the difference between the ^{14}*N*- and ^{15}*N*-MEEP polymers with respect to the P═N bond and how these differences change with increasing lithium concentration. At high Li concentrations, the labeled and unlabeled polymers appear to be nearly identical with respect to the P═N bonding. This is an indication of a dramatic change in the P═N interactions likely resulting from association of a Li^+ with the lone pair of electrons on the N.

An interesting observation from the Raman spectra of the ^{14}*N*-MEEP and ^{15}*N*-MEEP is that there were no obvious differences. This leads to the conclusion that many of the expected vibrations associated with P−N bonding as identified with model compounds[33−36] do not appear to be Raman active, at least not in MEEP, and the spectrum is dominated by the vibrational modes of the side chains. The only difference found in the spectra that could be associated with P−N bonding was found in the peak at 625 cm^{-1} which is apparently a combination of a P−N bending mode[34,36] and a P−O mode.[29] The shift due to the P−N bond can readily be seen in the spectra of the neat ^{14}*N*-MEEP and ^{15}*N*-MEEP (Figure 14). The shape of the peak in the ^{14}*N*-MEEP spectrum is skewed and simple peak fitting indicates that this band may actually be composed of at least two bands. One band is centered at ∼634 cm^{-1} and one at ∼625 cm^{-1}, and these bands are result from the P−N and P−O vibrations.[29] Increasing lithium concentrations tend to shift the peak to higher frequencies without significant band broadening. One interpretation of this is that the band is due solely to vibrations of the P−N bond and therefore interaction of Li with

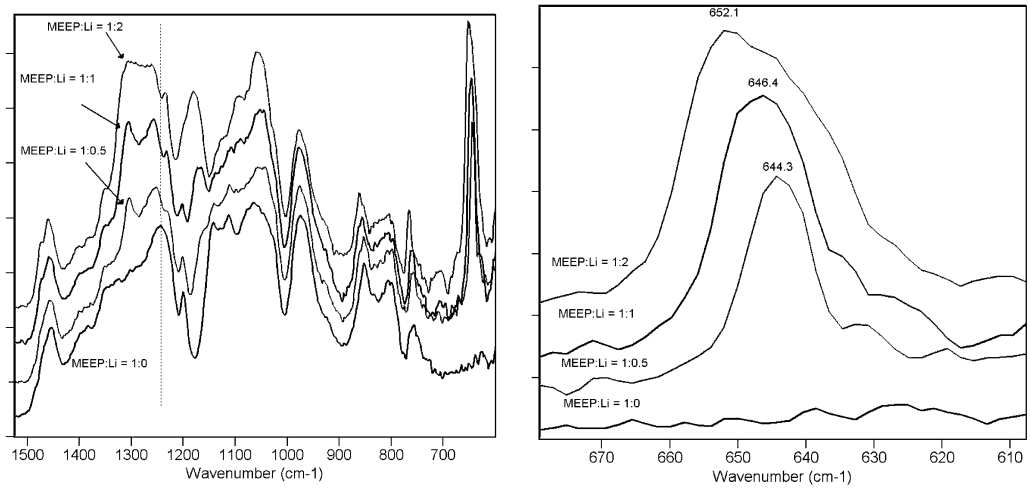

Figure 12. (a) Photoacoustic infrared spectra of MEEP with MEEP:Li ratios of 1:0, 1:0.5, 1:1, and 1:2. (b) Expanded region of the SO_3 absorption band of triflate.

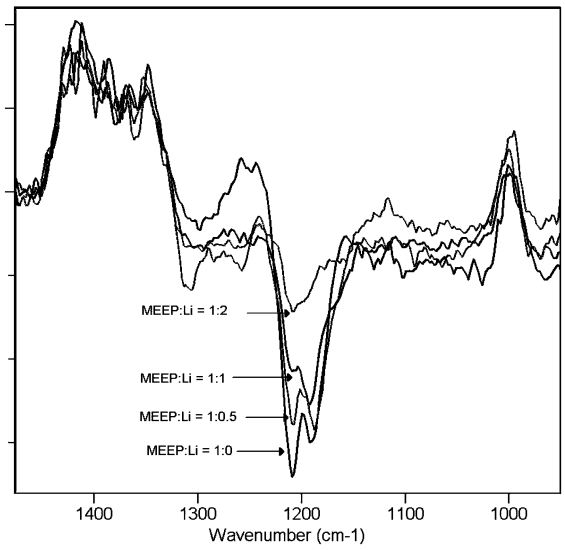

Figure 13. Photoacoustic infrared spectra of MEEP ratioed to ^{15}N-MEEP in the range of the P═N stretch at MEEP:Li ratios of 1:0, 1:0.5, 1:1, and 1:2 (i.e., MEEP:Li at 1:0 ratioed to ^{15}N-MEEP:Li at 1:0, MEEP:Li at 1:0.5 ratioed to ^{15}N-MEEP:Li at 1:0.5, etc.).

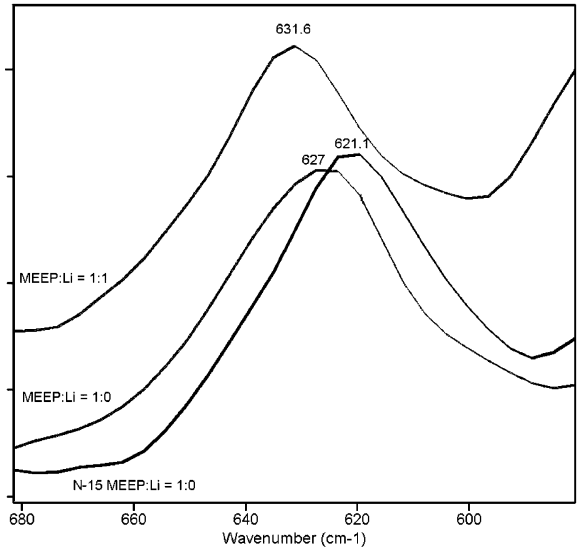

Figure 14. FT-Raman spectra of MEEP and ^{15}N-MEEP in the region of P−N and P−O vibrations of the polymer background.

the N in the background is the cause of the shift. A second interpretation is that the P−N and P−O vibrations are both affected by the addition of the cation. Both interpretations would be consistent with a coordination structure with the formation of a "pocket" involving lithium, N, and the P−O oxygens.

Molecular Dynamics Simulations. The molecular dynamics simulations[37] were performed with the COMPASS force field.[38−42] First, two 20-mer chains of MEEP were generated in a periodic box with a density of 1.0 g/cm^3 (experimental density at room temperature is 1.2 g/cm^3) and initial angles from the rotational isomeric state (RIS) model. The chains were then relaxed with an average temperature of 600 K for more than a nanosecond using microcanonical dynamics. The dynamics (advanced by the Verlet leapfrog algorithm[37]) required a time step size of 0.5 fs for energy conservation. Configurations were saved every hundredth step (0.05 ps). For the last 400 ps of equilibration, the velocities were rescaled if the temperature average for 0.5 ps deviated by more than 15 K in either direction. The average pressure near the end of the equilibration was about 800 bar. To increase the motion of the lithium, these simulations are run at a higher temperature than the experiment (600 K vs room temperature) and a lower density than experiment (1.0 g/cm^3 vs 1.2 g/cm^3).

Direct simulation of the lithium diffusion is not useful due to the strong binding of the ion with the polymer, and consequent low diffusivity, even at the elevated temperature employed.[43] Instead, after the initial equilibration stage, the polymer was simulated without the lithium ion for 236 ps with the same conditions as for the equilibration while instantaneous polymer configurations were selected. Since the main question of interest is the mean location of the lithium with respect to the different types of atoms in the polymer, it was deemed more efficient to keep the polymer motionless, insert the lithium ion in various starting positions, give it a random initial velocity, and determine the final position of the lithium ion. The freezing of the polymer is an approximation; however, the polymer dynamics are so slow (after 500 ps, the center of mass root-mean-squared displacement is less than 2 Å), that freezing the polymer is not likely to affect lithium ion dynamics on this time scale.

A working hypothesis was that the charges on the polymer determine the lithium position. A feature of the model used is

that atomic partial charges are calculated based on bonded interactions and thus are fixed throughout a simulation. Quantum mechanical density functional theory calculations were carried out on a small fragment of MEEP with a lithium ion, and found that the partial charges should change as a function of relative position between lithium and polymer atoms. Since the partial charges in the COMPASS force field remained constant during a given molecular dynamics simulation, it was decided to test whether the lithium will retain a specific position for different charge distributions. Three cases were considered:

1. All the partial charges on the polymer were assigned by the bond charge increment method employed in COMPASS,[38−42] and the lithium ion is given a charge of +1.

2. The partial charges on the phosphorus and nitrogen atoms were set to zero. All other partial charges remained the same as assigned by bond charge increment and the lithium ion remained at +1 charge.

3. The phosphorus and nitrogen partial charges were set to zero, all other polymer partial charges were the same as assigned by bond charge increment, and the lithium charge was set to +0.7.

Canonical dynamics using the Nosé−Hoover temperature control[44] with a relaxation time of 0.1 ps were performed for 350−750 ps, with the MEEP atoms frozen and only the lithium ion allowed to move. The lithium ion was placed near the backbone and a run for each of the three cases was performed from the same initial starting conditions. This was done for two polymer configurations separated by 236 ps of microcanonical dynamics.

In all six runs, the ion remained near the backbone. It moved within a small volume, but did not display the "hopping" or large-scale movement characteristic of small molecule diffusion. This was determined not to be a free volume problem as both helium and lithium atoms showed Fickian diffusion through the same fixed polymer configuration. The ions did not all finish in exactly the same position in the polymer, although they found places that had similar features. The preferred features are a "pocket" formed by the nitrogen of the backbone and some inner oxygens. The case 2 and case 3 runs had ions that tended to travel slightly farther than the case one runs (on average, about two mers farther); however, all were still coordinated with the backbone, the first oxygens, and much less often the second oxygens on the branches. The zero charge on the phosphorus and the nitrogen runs show the lithium slightly closer to the nitrogen. The ion did not move to be coordinated between the second and third oxygens on the branches.

Since the ion moved only small amounts when placed near the backbone, starting positions for the ion at the ends of the branches between the polymer chains were tried next with all three cases in order to gauge effect of initial placement. Although initially coordinated with the third oxygen on the branches of two mers, in all three cases, the lithium ion traveled to the backbone to be coordinated with nitrogen and a first branch oxygen. The values for the first peak in the ion−atom pair distribution functions (atom = oxygen or nitrogen) are in Table 2 for all nine runs.

In some cases, the ion appeared to end up closer to the oxygen atoms than the nitrogen. Nevertheless, the first oxygen is near the backbone, so further investigation was required to discriminate between first and subsequent oxygens in the pendant groups. Therefore, the lithium ion was randomly placed and several short canonical runs (15 ps) were performed under Case 1 conditions with a frozen polymer configuration. The ions were given a random initial velocity and tracked for ending position and mean-squared displacement. From a sample of 60 tests, thirty runs have mean-squared displacements of more than 5 Å^2. Of those that had significant displacement, only five runs finished unambiguously at the ends of branches with the third oxygen and its carbons as the nearest neighbors. Five other runs did have the third oxygen within a distance 3−4 Å due to branch bending, but were also associated with atoms near the backbone. Seventeen of the runs with significant ionic displacement finished with the first oxygen as a nearest neighbor. Six of these runs were also associated with nitrogen within 4 Å and another run had nitrogen as its closest neighbor. Ten of the mobile runs finished with both first and second oxygen as nearest neighbors.

TABLE 2: Position of the First Peaks in the Pair Distribution Functions (in Ångstroms)

	start near backbone								
	configuration 1			configuration 2			start near ends		
	case 1	case 2	case 3	case 1	case 2	case 3	case 1	case 2	case 3
nitrogen	2.5	2.4	2.4	2.5	2.1	2.2	2.5[b]	2.2	2.1
oxygen	2.9[a]	1.9	2.0	3.7[b]	1.9	2.0	3.7[b]	1.8	1.9

[a] A small peak is at 2.0 Å, but the first peak for $g(r) \geq 1$ is at 2.9 Å. [b] Very broad peak, this is the maximum.

Therefore, while it is possible for the lithium to be anywhere in the polymer, the preferred situation is to be coordinated with several atoms. This is similar to the simulation results found for lithium ions in poly(ethylene oxide).[45] Since this association is more likely near the backbone due to the nitrogen and oxygen arrangements, the lithium ion prefers to be near the backbone, even apart from the magnitude of the charge on the nitrogen.

Conclusion

NMR (^{1}H, ^{13}C, ^{15}N, and ^{31}P), IR, and Raman spectroscopies and molecular dynamic simulations examining LiOTf complexes of ^{15}*N*-MEEP and ^{15}*N*-HPP were performed. The analyses of these studies provide a more thorough understanding of the interactions of the lithium ion with the polymer regarding ionic transport in the polymer matrix. The mechanism proposed in the literature for ionic transport in MEEP states that lithium ion association was limited to the oxygen nuclei on the etherial pendant groups. Our results, experimentally and computationally, show that lithium ion association also occurs with the nitrogen nuclei of the polymer backbone. The molecular dynamic simulation models were designed to provide the best possible case for facilitating lithium ion movement in the polymer matrix, utilizing higher temperature and lower polymer density. These models concur with previous computational analyses that show while it is possible for lithium ion to be anywhere in the matrix, the preferred site for association is where it can be coordinated with several atoms. According to the model, this situation occurs when the lithium ion fits into the "pocket" formed by the backbone nitrogen nuclei and the oxygen nuclei of the pendant groups.

Experimental evidence for this "pocket" is observed in the vibrational and NMR spectroscopic data of lithium complexes of MEEP and ^{15}*N*-MEEP. The isotope labeling of the polymers is readily observed in the spectra. Differences in the P−N stretching and P−O bending modes associated with lithium ion interactions with the polymer matrix are observed by changes in the IR and Raman spectra. The interpretations are consistent with lithium ion association with the nitrogen nuclei of the backbone and the oxygen nuclei of the pendant groups.

The NMR data for these lithium complexes indicate that the polymer-salt interactions are sensitive to the selection of the

solvent. When THF-d_8 was used, the interactions between the solvent and the salt dominated those between the salt and the polymer. By utilizing a noncoordinating solvent (such as $CDCl_3$), reliable ^{13}C, ^{15}N, and ^{31}P NMR data regarding chemical shift and the T_{1min} values that are the result of salt−polymer interactions were obtained. Utilizing ^{15}N-labeled polyphosphazenes afforded us the direct observation of lithium ion coordination to the polymer backbone by NMR spectroscopy. The NMR data of the carbon resonances of ^{15}N-MEEP agree with the previously published transport mechanism that the oxygen nuclei are also involved with lithium ion complexation. Changes in the chemical shifts in the ^{15}N and ^{31}P NMR spectra of ^{15}N-MEEP and ^{15}N-HPP following lithium ion addition suggest that the nitrogen nuclei of the polyphosphazene backbone have a significant role in ion complexation and mobility. The NMR data for ^{15}N-HPP indicate that the solvation energies of the less polar MeOP and *o*-AL pendant groups are not sufficient to successfully compete with the MEE pendant groups for complexation with the lithium ion. The NMR data strongly indicate that the observed downfield shift of resonance E in the ^{15}N NMR spectrum is due to lithium ion complexation with the backbone nitrogen nuclei. Most significantly, the sharp decrease in the ^{15}N NMR T_{1min} value measured for ^{15}N-MEEP is consistent with the association of lithium ion with the nitrogen nuclei of the polymer backbone.

Acknowledgment. The authors thank Dr. Tom Pratum for his assistance with the Bruker DMX 750 NMR Spectrometer at the University of Washington. This work was supported by the United States Department of Energy through contract DE-AC07-99ID13727.

References and Notes

(1) Ratner, M. A.; Shriver, D. F. *Chem. Rev.* **1988**, *88*, 109−124.
(2) Blonsky, P. M.; Shriver, D. F.; Austin, P.; Allcock, H. R. *J. Am. Chem. Soc.* **1984**, *106*, 6854−6855.
(3) Fenton, D. E.; Parker, J. M.; Wright, P. V. *Polymer* **1973**, *14*, 589−589.
(4) Berthier, C.; Gorecki, W.; Minier, M.; Armand, M. B.; Chabagno, J. M.; Rigaud, P. *Solid State Ionics* **1983**, *11*, 91−95.
(5) Lonergan, M. C.; Shriver, D. F.; Ratner, M. A. *Electrochim. Acta* **1995**, *40*, 2041−2048.
(6) Rhodes, C. P.; Frech, R. *Solid State Ionics* **1999**, *121*, 91−99.
(7) Rhodes, C. P.; Kiassen, B.; Frech, R.; Dai, Y.; Greenbaum, S. G. *Solid State Ionics* **1999**, *126*, 251−257.
(8) Allcock, H. R.; Napierala, M. E.; Olmeijer, D. L.; Best, S. A.; Merz, K. M. *Macromolecules* **1999**, *32*, 732−741.
(9) Stewart, F. F.; Singler, R. E.; Harrup, M. K.; Peterson, E. S.; Lash, R. P. *J. Appl. Polym. Sci.* **2000**, *76*, 55−66.
(10) Wisian-Neilson, P.; Garcia-Alonso, F. J. *Macromolecules* **1993**, *26*, 7156−7160.
(11) Walker, C. H.; St John, J. V.; Wisian-Neilson, P. *J. Am. Chem. Soc.* **2001**, *123*, 3846−3847.
(12) Allcock, H. R.; Fitzpatrick, R. J.; Salvati, L. *Chem. Mater.* **1991**, *3*, 1120−1132.
(13) Tang, H.; Pintauro, P. N.; Guo, Q. H.; O'Connor, S. *J. Appl. Polym. Sci.* **1999**, *71*, 387−399.
(14) Allen, R. W.; Obrien, J. P.; Allcock, H. R. *J. Am. Chem. Soc.* **1977**, *99*, 3987−3991.
(15) Harrup, M. K.; Stewart, F. F. *J. Appl. Polym. Sci.* **2000**, *78*, 1092−1099.
(16) Van Geet, A. L. *Anal. Chem.* **1970**, *42*, 679−680.
(17) Petrowsky, M.; Rhodes, C. P.; Frech, R. *J. Solution Chem.* **2001**, *30*, 171−181.
(18) Alia, J. M.; Edwards, H. G. M. *Vib. Spectrosc.* **2000**, *24*, 185−200.
(19) ^{15}N-ammonium sulfate: ^{15}N 98%+, Cambridge Isotope Laboratories.
(20) Allen, C. W.; Hneihen, A. S.; Peterson, E. S. U.S. Patent 6309619, 2001.
(21) Allen, C. W.; Hneihen, A. S. *Phosphorus, Sulfur Silicon Relat. Elem.* **1999**, *146*, 213−216.
(22) Stewart, F. F.; Harrup, M. K.; Luther, T. A.; Orme, C. J.; Lash, R. P. *J. Appl. Polym. Sci.* **2001**, *80*, 422−431.
(23) Mark, J. E.; Allcock, H. R.; West, R. *Inorganic Polymers*; Prentice Hall: Englewood Cliffs, NJ, 1992.
(24) Krajewski-Bertrand, M.-A.; Lauprêtre, F.; Monnerie, L. *Dynamics of Solutions and Fluid Mixtures by NMR*; John Wiley & Sons: Chichester, 1995.
(25) Günther, H. *NMR Spectroscopy: Basic Principles, Concepts, and Applications in Chemistry*, 2nd ed.; John Wiley & Sons: Chichester, 1995.
(26) Desrosiers, P. J.; Cai, L. H.; Lin, Z. R.; Richards, R.; Halpern, J. *J. Am. Chem. Soc.* **1991**, *113*, 4173−4184.
(27) Allcock, H. R.; Napierala, M. E.; Cameron, C. G.; O'Connor, S. J. M. *Macromolecules* **1996**, *29*, 1951−1956.
(28) Lerner, M. M.; Lyons, L. J.; Tonge, J. S.; Shriver, D. F. *Chem. Mater.* **1989**, *1*, 601−606.
(29) York, S.; Kellam, E. C.; Allcock, H. R.; Frech, R. *Electrochim. Acta* **2001**, *46*, 1553−1557.
(30) Fernandez, L. E.; BenAltabef, A.; Varetti, E. L. *Spectroc. Acta, Part A* **1996**, *52*, 287−296.
(31) York, S.; Frech, R.; Snow, A.; Glatzhofer, D. *Electrochim. Acta* **2001**, *46*, 1533−1537.
(32) Johansson, P.; Jacobsson, P. *J. Phys. Chem. A* **2001**, *105*, 8504−8509.
(33) Painter, P. C.; Zarian, J.; Coleman, M. M. *Appl. Spectrosc.* **1982**, *36*, 265−271.
(34) Bougeard, D.; Bremard, C.; Dejaeger, R.; Lemmouchi, Y. *J. Phys. Chem.* **1992**, *96*, 8850−8855.
(35) Dumont, D.; Bougeard, D. *Comput. Theor. Polym. Sci.* **1999**, *9*, 89−97.
(36) Elass, A.; Dhamelincourt, P.; Becquet, R.; Vergoten, G. *J. Mol. Struct.* **1996**, *384*, 41−54.
(37) Allen, M. P.; Tildesley, D. J. *Computer Simulations of Liquids*; Cambridge University Press: Cambridge, 1989.
(38) COMPASS is distributed by Accelrys (formerly Molecular Simulations, Inc.).
(39) Sun, H. *J. Phys. Chem. B* **1998**, *102*, 7338−7364.
(40) Sun, H.; Ren, P.; Fried, J. R. *Comput. Theor. Polym. Sci.* **1998**, *8*, 229−246.
(41) The van der Waals interactions used the following spline cutoff

$$S = \frac{(r_{off} - r_{ij}^2)^2(r_{off}^2 + 2r_{ij}^2 - 3r_{on}^2)}{(r_{off}^2 - r_{on}^2)^3} \qquad r_{on}^2 < r_{ij}^2 < r_{off}^2$$

with a spline-on distance of 9 Å and a spline-off distance of 12 Å in the cubic box of length 26.6 Å. The Coulombic interactions were calculated with Ewald sums.
(42) *Force field-Based Simulations*; Molecular Simulations, Inc.: San Diego, April 1999.
(43) A single lithium ion, with a volume equal to that of the loading of 4.2 monomers/lithium and with a polymer density of 1 g/cm^3 at the maximum experimental specific conductivity (about 50×10^{-6} S/cm at about 300 K), has a diffusion constant of only 2×10^{-9} cm^2/s (2×10^{-5} Å^2/ps), using the Nernst−Einstein relation.
(44) Hoover, W. G. *Phys. Rev. A* **1985**, *31*, 1695−1697.
(45) Muller-Plathe, F.; van Gunsteren, W. F. *J. Chem. Phys.* **1995**, *103*, 4745−4756.